chemosensors

MDPI

Article

Phthalocyanine-Carbon Nanotube Hybrid Materials: Mechanism of Sensor Response to Ammonia from Quantum-Chemical Point of View

Pavel Krasnov [1], Victoria Ivanova [2], Darya Klyamer [2], Aleksandr Fedorov [1,3] and Tamara Basova [2,*]

[1] International Research Center of Spectroscopy and Quantum Chemistry, Siberian Federal University, 26 Kirensky st., 660074 Krasnoyarsk, Russia
[2] Nikolaev Institute of Inorganic Chemistry SB RAS, 3 Lavrentiev Pr., 630090 Novosibirsk, Russia
[3] Kirensky Institute of Physics, Federal Research Center KSC SB RAS, 50/38 Akademgorodok, 660036 Krasnoyarsk, Russia
* Correspondence: basova@niic.nsc.ru

Abstract: Quantum chemical calculations of the geometric and electronic structure of periodic hybrid compounds representing carbon nanotubes (10,0) with zinc phthalocyanine molecules ZnPc-*x*py (x = 0, 1, 2, 4) on their surface and their interaction with ammonia were carried out to explain the dependence of the sensor response of the hybrid materials to ammonia on the number of substituents in the ZnPc-*x*py macrocycle and to clarify the nature of the interaction between ammonia and phthalocyanine molecules. It was found that the key feature of these materials, which determines their sensor response toward ammonia, is the presence of an impurity band in the band gap of a carbon nanotube, formed by the orbitals of macrocycle atoms. When ammonia adsorbs through the formation of hydrogen bonds with the side atoms of phthalocyanine, the energy of this impurity band decreases. As a consequence, the electron population of the conduction band and, accordingly, the electrical conductivity of the hybrid materials become lower. Moreover, with an increase in the number of oxypyrene substituents in ZnPc-*x*py, the interaction energy of ammonia increases and, as a result, the decrease in the energy of the impurity band becomes higher. These facts may explain recent experimental measurements of the parameters of the sensor response of similar hybrid materials to ammonia, where, in particular, it was shown that the sensor response is reversible, and its value increases with an increase in the number of oxypyrene substituents in the phthalocyanine macrocycle.

Keywords: metal phthalocyanine; carbon nanotubes; quantum-chemical calculations; ammonia sensors

Citation: Krasnov, P.; Ivanova, V.; Klyamer, D.; Fedorov, A.; Basova, T. Phthalocyanine-Carbon Nanotube Hybrid Materials: Mechanism of Sensor Response to Ammonia from Quantum-Chemical Point of View. *Chemosensors* **2022**, *10*, 479. https://doi.org/10.3390/chemosensors10110479

Academic Editor: Filippo Giubileo

Received: 24 October 2022
Accepted: 11 November 2022
Published: 14 November 2022

1. Introduction

In the last decade, carbon nanotubes (CNT) and hybrid materials with various classes of compounds have been the subjects of numerous theoretical and experimental studies [1]. Their electrophysical characteristics and the ability to change the conductivity in the atmosphere of various gases contribute to their widespread use as active layers of chemiresistive sensors of various gases and some liquids [1–3]. Covalent and non-covalent functionalization by metal or metal oxide nanoparticles, polymers, and various aromatic molecules are widely used to improve sensor characteristics such as sensitivity and selectivity with respect to various gases [2,4–6]. The advantage of non-covalent functionalization over covalent interactions is minimal damage to the single-walled CNT surface with less distortion in their electronic structure [7,8]. Among other aromatic molecules, metal phthalocyanines (MPc), which have an extended π-system and the ability to vary widely in chemical structure, are promising candidates

for the modification of carbon nanotubes by non-covalent functionalization [9]. The expansion of the MPc aromatic system, when passing from phthalocyanine to naphthalocyanine (MNc) [10] or by introducing additional aromatic substituents into the macroring [11,12], was shown to improve the interaction between the MPc macrocycle and CNTs and, thus, to lead to an improvement in the chemiresistive sensor performance.

The literature abounds with examples of the use of CNT/MPc hybrid materials as active layers of gas sensors for the determination of chlorine [13,14], NO_2 [15], ammonia [16–18], and some other gases and volatile organic vapors [19]. At the same time, an analysis of the literature shows that systematic studies of the influence of the phthalocyanine structure (for example, the type of substituents) on sensor characteristics, as well as studies of the nature of the interaction of hybrid materials with analytes and the mechanism of the sensor response, are sporadic [20,21]. Most researchers, referring to each other, give only a speculative description of the mechanism based on the charge transfer between the electron acceptor or electron donor analyte molecules and a phthalocyanine molecule adsorbed on the surface of CNTs, which leads to an increase or decrease in the number of charge carriers, resulting in a change in the resistance of a sensing hybrid film [22–25]. Such conclusions usually are not supported by either experimental studies or theoretical calculations.

It has been shown in our previous works that CNT/MPc hybrid materials demonstrated a high sensor response to ammonia [9,10,26,27]. The limit of ammonia detection of the CNT/MPc-based sensors was found to reach 0.4 ppm and their sensitivity to ammonia was much higher than to CO_2, H_2, H_2S, CH_4, ethanol, acetone, and dichloromethane vapors. For this reason, the nature of the interaction of hybrid materials with ammonia is considered in this work.

The process of adsorption of oxygen molecules on the surface of a hybrid material or phthalocyanine film during exposure to ambient air with the formation of O_2^- species and their further reaction with reducing gases such as ammonia is also considered as a mechanism. In this connection, some researchers indicate that the following reaction proceeds: $4NH_3(g) + 3O_2^-(ads) \rightarrow 2N_2(g) + 6H_2O(g) + 6e^-$ [28,29], while the authors of other works [30,31] believe that the reaction with the formation of NO ($4NH_3(g) + 5O_2^-(ads) \rightarrow 4NO(g) + 6H_2O(g) + 5e^-$) is more preferable. Electrons release during these processes and rapidly transfer to the carbon nanomaterials, changing their resistance.

Another point of discussion when considering the mechanism of the sensor response is the question of the adsorption sites of the analyte molecules on the surface of a hybrid material. DFT calculations are the most useful tool to clarify this issue. In most works [18,22,32–36], the interaction of the analyte molecules through the central metal is considered. For example, to explain the dependence of the sensor response on the nature of the central metal, Li et al. [22] estimated the binding energy in MPc-NH_3 systems depending on M, which decreased in the order of Co > Cu > Ni > Fe from 21.7 to 6.2 kcal/mol. Comparable values of the binding energies were also obtained in the works of other authors [35]. Guo et al. [28] investigated the effect of substituents in CoPcs bearing various phenoxyl substituents in their hybrids with reduced graphene oxide on the sensor response to ammonia. It was shown that the binding energies between NH_3 and CoPc bearing various phenoxyl substituents varied in the range of 21.7–23.1 kcal/mol.

On the one hand, the analysis of the interaction of ammonia through the central metal in those works showed that the central metal played a critical role in NH_3 sensitivity. Thus, this consideration raises several ambiguous points. Firstly, the values of the binding energy of NH_3 with some central metals indicate a rather strong binding. With such an interaction, the sensor response could hardly be reversible, which contradicts experimental data showing that hybrid materials and metal phthalocyanine films demonstrate a completely reversible sensor response at room temperature [17,37]. Secondly, the consideration of the interaction of NH_3 with the metal centers is acceptable only if there is direct access to the central metal in the MPc molecules. This is possible, for example, if the phthalocyanine molecules are deposited as a monolayer on the surface of

a substrate or nanotubes, and the neighboring molecules or nanotubes do not prevent access to them. If the phthalocyanine molecules are packed in stacks on the CNT surface or in polycrystalline films, such a consideration is doubtful, since the separation between the neighboring molecules in the stack is 3.3–3.4 A, which is insufficient for the free penetration of an NH_3 molecule to the central atom. In this case, the consideration of the interaction of the analyte molecules with a phthalocyanine molecule through the edge atoms of the MPc macrocycle or substituents in the ring seems more appropriate. Moreover, Chia et al. [15], in their experimental studies of the interaction between ammonia and CuPc by the methods of in-situ X-ray absorption spectroscopy (XAS) and EXAFS, demonstrated that the first derivative of XANES did not confirm the coordination of NH_3 with the Cu metal center. Therefore, it was proposed to consider the interaction of NH_3 with the benzene ring or the bridging nitrogen atom of the macrocycle.

We have already used a similar explanation in our recent work [38] when explaining the effect of the number (x = 0, 1, 2, 4) of oxypyrene (py) substituents in zinc(II) phthalocyanine molecules ZnPc-$x$py-h on the sensor properties of their hybrid materials with single-walled carbon nanotubes. In particular, it was shown that the chemiresistive sensor response to ammonia increased in the order ZnPc-0py-h < ZnPc-1py-h < ZnPc-2py-h < ZnPc-4py-h. To explain this regularity, we considered three possible sites for NH_3 molecule adsorption: the central metal atom, oxypyren substituents, and side phthalocyanine atoms. Quantum-chemical calculations of these means of ammonia interaction with CNT(10,0)/ZnPc-$x$py hybrid systems have shown that, in the first case, the binding energy was too high (more than 0.8 eV) for ammonia desorption under normal conditions, which could not explain the reversibility of the sensor response. In the case of the oxypyren substituent, the interaction of the NH_3 molecule was too weak (about 0.14 eV) to change the electron structure of the hybrid materials significantly and, as a result, their conductivity. When the ammonia molecules interacted with the side phthalocyanine atoms, the binding energy was enough (about 0.24 eV) to decrease the energy of the impurity electron band of the hybrid structures. This led to a lower population of the conduction band and, as a result, to a decrease in the electrical conductivity. Moreover, this decrease was higher the greater the number of oxypyren substituents, which explained the experimental observations. Despite the used explanation of the experimental results, several questions remained unresolved, namely, the nature of the impurity electron band, the dependence of its energy change on the number of oxypyren substituents, and the influence of these substituents on the binding energy of ammonia. Therefore, this work is aimed at clarifying these issues.

In this paper, we show using quantum chemical calculations that the impurity electron band in the band gap of the CNT(10,0)/ZnPc-$x$py hybrid structures is formed by the orbitals of the phthalocyanine atoms. The interaction of the NH_3 molecules with the side atoms of phthalocyanine occurs via the formation of hydrogen bonds. The presence of the oxypyren substituents leads to the strengthening of these bonds due to the macrocycle polarization. A stronger interaction of the ammonia molecules with phthalocyanine leads to a more significant decrease in the impurity band energy.

2. Objects and Methods of Investigation

Quantum-chemical calculations of the geometric and electronic structure of the CNT(10,0)/ZnPc-$x$py hybrid compounds, where x = 0, 1, 2, and 4, were performed using the SCC-DFTB method in the DFTB+ software package [39,40]. The 3OB parameter set (Slater-Koster files) was used to describe the interatomic interaction [41,42]. The dispersion interaction was corrected using the DFT-D3 method [43,44].

Each compound was considered as a periodic structure, the unit cell of which contained a fragment of a carbon nanotube (10,0) 12a long, where a is the unit cell length of pure CNT(10,0), with a ZnPc-$x$py molecule on the surface (Figure 1). The orientation of phthalocyanine in each case was chosen so that the total energy of the entire system was minimal due to the greater overlap of the conjugated π-systems of the macrocycle and the

carbon surface [12,45]. In this case, the periodicity of the hybrid was considered along the CNT(10,0) axis (direction *c*), and vacuum gaps of at least 50 Å were set along the other two perpendicular directions *a* and *b* in order to exclude the interaction of the hybrid with its images in neighboring cells.

The first Brillouin zone was divided according to the Monkhorst–Pack scheme [46] into a grid containing 1 × 1 × 15 *k*-points along the directions *a*, *b*, and *c*, respectively. The optimization of the geometric structure of the compounds under consideration was carried out up to the value of the forces acting on atoms equal to 1×10^{-4} a.u. In this case, since the number of electrons in the case of all the considered systems, including the carbon nanotube and phthalocyanines separately, was even, the calculations were carried out without taking into account spin polarization.

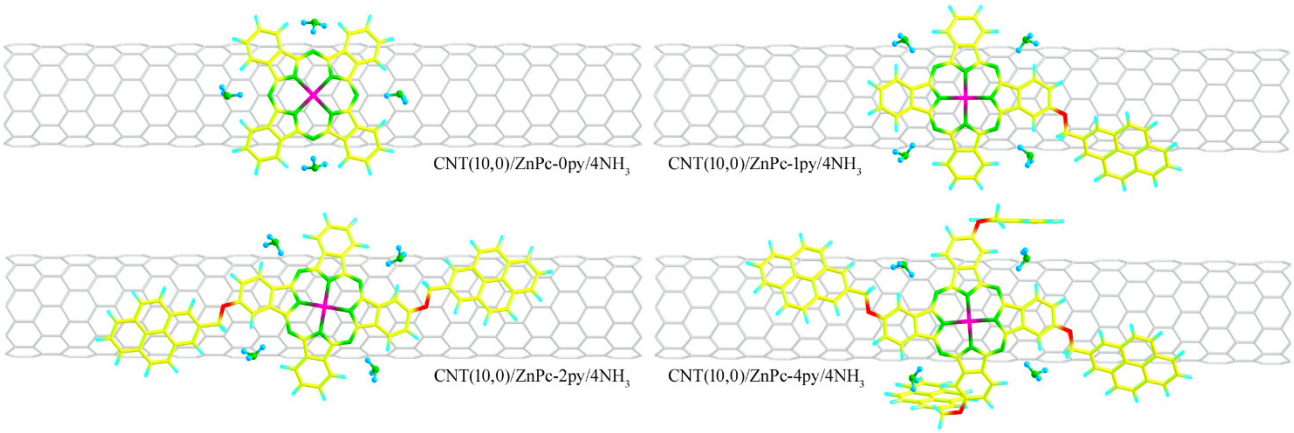

Figure 1. Geometrical structures of CNT(10,0)/ZnPc-*x*py/4NH3 obtained as a result of quantum-chemical modeling by the SCC-DFTB method.

In the first step, the geometric structures of the CNT(10,0)/ZnPc-*x*py hybrids were optimized, during which both the position of all the atoms and the cell length along the periodicity axis were varied. In the second step, four NH3 molecules were added to each structure so that they interacted with the side atoms of the phthalocyanines. Furthermore, in the obtained CNT(10,0)/ZnPc-*x*py/4NH3 structures, the geometry and position of the ammonia molecules were optimized at fixed positions of the atoms and the sizes of the hybrid structures themselves (Figure 1). As a result, data on the electronic structure (band structure and density of states) of the CNT(10,0)/ZnPc-*x*py hybrids were obtained before and after the addition of the four NH3 molecules.

To describe the nature and features of the interaction of ammonia with the considered phthalocyanine molecules, additional quantum-chemical calculations of the geometric and electronic structure of ZnPc-*x*py molecules with the four NH3 molecules were carried out. The orientation of the latter was chosen similarly to that obtained by considering the CNT(10,0)/ZnPc-*x*py/4NH3 hybrid structures (Figure 2). Since the number of electrons here was even in all cases, spin polarization as well as any symmetry constraints were not considered.

At the stage of the geometry optimization of the ZnPc-*x*py/4NH3 aggregates, calculations were performed using the DFT BP86-D3/def2-SVP method [43,44,47–49] in the ORCA software package [50,51] using RI approximation [52–57] and the corresponding Def2/J auxiliary basis set [58]. Then, the binding energy E_b of each ammonia molecule in the composition of each aggregate was calculated from the difference in the total energies of the corresponding structure and its components, the geometries of which were also optimized separately:

$$E_b = E_{\mathrm{NH_3}} + E_{\mathrm{ZnPc-}x\mathrm{py/3NH_3}} - E_{\mathrm{ZnPc-}x\mathrm{py/4NH_3}} - \Delta E_{\mathrm{BSSE}}, \quad (1)$$

where ΔE_{BSSE} is the correction to the binding energy, taking into account the basis set superposition error, which, in turn, was estimated as follows:

$$\Delta E_{\mathrm{BSSE}} = (E^{\mathrm{ZnPc-}x\mathrm{py/4NH_3}}_{\mathrm{ZnPc-}x\mathrm{py/3NH_3}} + E^{\mathrm{ZnPc-}x\mathrm{py/4NH_3}}_{\mathrm{NH_3}}) - (E^{\mathrm{ZnPc-}x\mathrm{py/4NH_3}}_{\mathrm{ZnPc-}x\mathrm{py/3NH_3^*}} + E^{\mathrm{ZnPc-}x\mathrm{py/4NH_3}}_{\mathrm{NH_3^*}}). \quad (2)$$

Here, the superscript ZnPc-*x*py/4NH$_3$ indicates that the geometries of ZnPc-*x*py/3NH$_3$ and NH$_3$, respectively, were taken from an optimized aggregate of a phthalocyanine molecule and four ammonia molecules, while their geometry optimization was not performed, but only the calculation of the total energy was carried out. An asterisk in the subscript means that the specified fragment of the whole aggregate was considered in the case when the atoms of the second fragment were dummy; that is, they were points described by the corresponding basis sets of atomic orbitals.

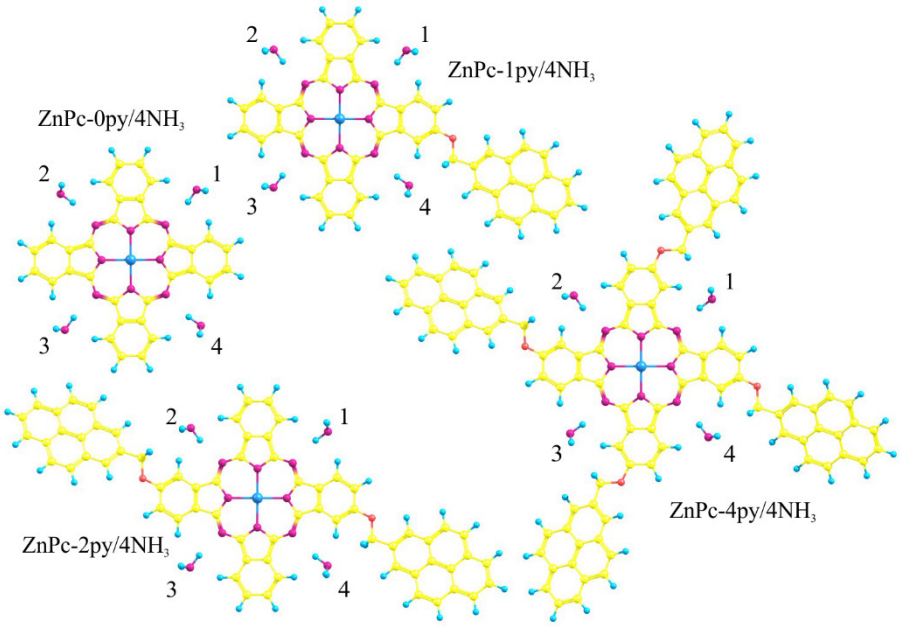

Figure 2. Geometrical structures of ZnPc-*x*py/4NH$_3$ aggregates, obtained from the results of quantum-chemical calculations by the DFT BP86-D3/def2-SVP method. The numbers 1–4 indicate the order of calculation of the binding energy of the corresponding NH$_3$ molecule in the composition of the entire aggregate.

In the next step, the electron wave functions of the optimized ZnPc-*x*py/4NH$_3$ compounds were calculated using the cc-pVTZ basis set of atomic orbitals [59]. In the framework of the QTAIM theory [60–62], a topological analysis of the electron density distribution $\rho(\mathbf{r})$ in the structures under consideration was performed using these wave functions and the AIMAll software package [63]. In this approach, the indicator of the binding interaction of two atoms is the presence of a bond critical point (3,−1) (BCP) between them. Here, $\omega = 3$ is the rank of the Hessian of $\rho(\mathbf{r})$ at this point, and $\sigma = -1$ is the sum of the signs of the Hessian eigenvalues λ_i ($\lambda_1 < 0$, $\lambda_2 < 0$, and $\lambda_3 > 0$).

Based on the set of values of these parameters, including the electron density Laplacian $\nabla^2\rho(\mathbf{r}) = \lambda_1 + \lambda_2 + \lambda_3$, it is possible to judge the nature of the interaction between the considered atoms. In particular, if $|\lambda_1|/\lambda_3 > 1$ ($\nabla^2\rho(\mathbf{r}) < 1$), the so-called "shared interaction" occurs, in which the accumulation and sharing of electron density in the interatomic space typical for covalent bonds are observed. In the case when $|\lambda_1|/\lambda_3 < 1$ ($\nabla^2\rho(\mathbf{r}) > 1$), a "closed-shell interaction" is observed, which is characteristic of ionic, high-polar covalent, hydrogen, and van der Waals bonds [60–63]. In this case, there is an outflow of electron density from the critical point toward atomic nuclei. There is also an "intermediate interaction", in which the value of $\nabla^2\rho(\mathbf{r})$ is also positive, but the chemical bond is considered covalent if the value of $\rho(\mathbf{r})$ is large.

3. Results and Discussion

After the optimization of the geometry of the CNT(10,0)/ZnPc-*x*py hybrids, as well as the geometry and arrangement of the four ammonia molecules bound to them through the side atoms of the phthalocyanines, calculations and analysis of the band structure and electron densities of the states of all the considered objects were performed (Figure 3). Here, first of all, it should be noted that the band gaps (E_{g1} and E_{g2}) of the hybrid materials under study, practically, do not depend either on the number of oxypyrene substituents in the zinc phthalocyanine macrocycle or on the presence of ammonia. The band gap values E_{g1} of the hybrids without the NH_3 molecules and E_{g2} of the hybrids with the NH_3 molecules differ only by thousandths of eV (Table 1). At the same time, considering the densities of the states (DOS) (Figure 3, central and right panels) and the visualization of the wave functions (Figure 3, left panels), it should be concluded that the conduction band bottom and the valence band top in all the structures are formed by the orbitals of the carbon atoms of CNT(10,0).

The most interesting point here is the presence in the band gap of an impurity band formed mainly by the orbitals of the phthalocyanine atoms. Since this band does not hybridize with other bands, the electrons populating it do not directly participate in electrical conduction. However, due to thermal excitation, they can pass into the conduction band of CNT, changing the electrical conductivity of the carbon nanotube. The key factor determining the possibility of this transition is the energy difference between the impurity band and the conduction band bottom.

In the case of hybrids without ammonia molecules, the value of ΔE_1 of this difference decreases with an increase in the number of oxypyrene substituents of zinc phthalocyanine (Figure 3). This may be due to an increase in the strength of the bond between the ZnPc-*x*py molecules and CNT(10,0) with an increase in *x*, which was demonstrated earlier [12]. When the four NH_3 molecules attach to the side atoms of phthalocyanine, the energy difference between the impurity band and the conduction band bottom increases to ΔE_2, which should be accompanied by a decrease in the electrical conductivity of the carbon nanotube.

Table 1. Band gap and change in the position of the impurity band and the conduction band population in CNT(10,0)/ZnPc-*x*py hybrids with the addition of four ammonia molecules.

x	E_{g1}, eV	E_{g2}, eV	ΔE, eV	n_1/n_2
0	0.774	0.774	0.005	1.10
1	0.774	0.773	0.013	1.29
2	0.775	0.774	0.019	1.45
4	0.772	0.772	0.038	2.10

The most important point is that the change in $\Delta E = \Delta E_2 - \Delta E_1$ during ammonia adsorption increases with an increase in the number of oxypyrene substituents in zinc phthalocyanine in the hybrid compound (Table 1). If we take into account that the population of the conduction band (n_1 without NH_3 molecules and n_2 with NH_3 molecules) depends on the energy of the electron transition into it, according to Equation (3),

$$n_1 \propto \exp\left(-\frac{\Delta E_1}{2kT}\right), \quad n_2 \propto \exp\left(-\frac{\Delta E_2}{2kT}\right), \tag{3}$$

where k is the Boltzmann constant, T is the temperature, then its decrease with the addition of the four NH_3 molecules can be estimated by the ratio 4:

$$\frac{n_1}{n_2} = \exp\left(-\frac{\Delta E_1}{2kT}\right) \Big/ \exp\left(-\frac{\Delta E_2}{2kT}\right) = \exp\left(\frac{\Delta E_2 - \Delta E_1}{2kT}\right) = \exp\left(\frac{\Delta E}{2kT}\right). \tag{4}$$

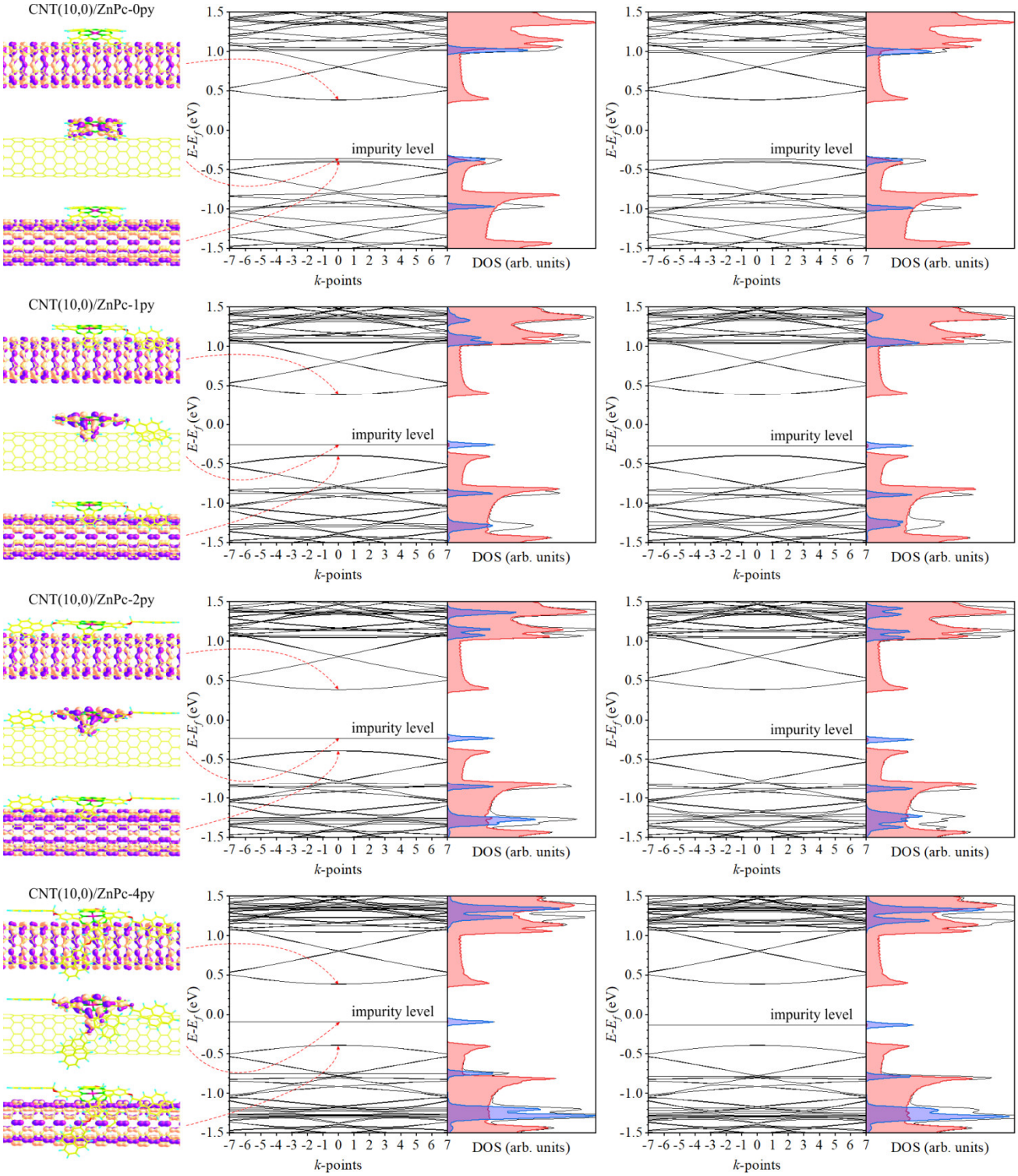

Figure 3. Band structure and densities of states of CNT(10,0)/ZnPc-*x*py (**center** panels) and CNT(10,0)/ZnPc-*x*py/4NH_3 (**right** panels); electron wave functions of the conduction band bottom, the impurity band, and the valence band top of the hybrids without ammonia molecules (**left** panels). In the case of densities of states, the black line is the total DOS, and the red and blue peaks are the partial DOS of the CNT(10,0) and ZnPc-*x*py atoms separately.

With an increase in the number of oxypyrene substituents, this ratio increases (Table 1). This means that the addition of ammonia leads to a greater decrease in the population of the conduction band. Thus, at room temperature, in the case of CNT(10,0)/ZnPc-0py, the population decreases by 1.1, while in the case of CNT(10,0)/ZnPc-4py, it decreases by

2.1. This, in turn, determines the sensitivity of the hybrid materials under consideration: the more oxypyrene substituents, the more the conduction band population decreases when the NH_3 molecules are added, the more the electrical conductivity decreases, and, as a result, the sensor response to ammonia increases, as was observed in earlier experimental studies [38].

A deeper downward shift of the indicated impurity level in the CNT(10,0)/ZnPc-*x*py hybrids in the case of the larger *x* values with the addition of the four NH_3 molecules may be caused by the fact that the strength of the interaction of ammonia with the side atoms of the phthalocyanine molecule increases with an increase in the number of oxypyrene substituents. In this case, the expected effect should be a stronger impact of ammonia on the electron system of the macrocycle. As a result of the quantum-chemical calculations of the ZnPc-*x*py/4NH_3 molecular systems using the DFT BP86-D3/def2-SVP method, it was shown that the introduction of oxypyrene substituents led to an increase in the binding energy of the ammonia molecule in the position adjacent to the attachment site (Table 2).

In particular, in the case of ZnPc-1py, the strongest binding is observed in position 4 (Figure 2), while in the case of ZnPc-2py, in positions 2 and 4. This is due to a shift in the electron density in the macrocycle due to the polarization action of the oxypyrene substituent. This effect is most clearly observed in the case of one substituent. If, in the ZnPc-0py/4NH_3 compound, the E_b values of all the NH_3 molecules are the same, then, in the ZnPc-1py/4NH_3 compound, they are all different. In positions **1** and **2**, they are lower than in position **4**. In this case, the average binding energy of the four ammonia molecules is higher in the case of ZnPc-1py/4NH_3 than in the case of ZnPc-0py/4NH_3. Similarly, the E_b values are higher in the case of phthalocyanine with the four oxypyrene substituents compared to phthalocyanine without the oxypyrene substituents.

Table 2. Binding energies (in eV) of each of the four NH_3 molecules in ZnPc-*x*py/4NH_3 aggregates.

x	**Position Number of the NH_3 Molecule (in Accordance with Figure 2)**			
	1	**2**	**3**	**4**
0	0.141	0.141	0.141	0.141
1	0.133	0.127	0.141	0.215
2	0.139	0.149	0.145	0.204
4	0.156	0.156	0.156	0.156

The obtained values of the binding energy of the NH_3 molecules are comparable with the energies of the hydrogen bonds. However, in order to obtain more reliable information about the nature of the interaction of ammonia with the side atoms of the phthalocyanines, the electronic structure of the ZnPc-xpy/4NH_3 aggregates was examined.

It was found that, as a result of the topological analysis of the electron density distribution in ZnPc-1py/4NH_3, performed within the framework of QTAIM, three critical bond points are formed between each NH_3 molecule and the side phthalocyanine atoms (Figure 4).

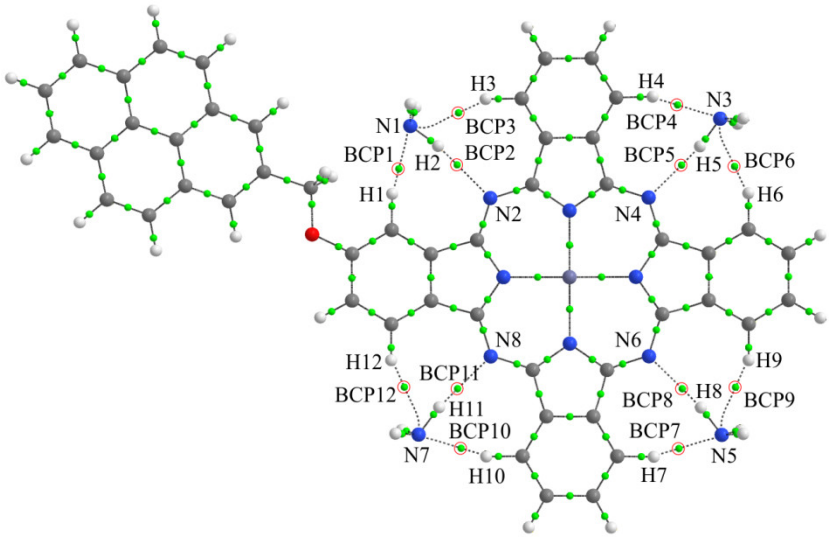

Figure 4. Bond critical points in the ZnPc-1py aggregate with four ammonia molecules (red circles show the BCP1-BCP12 points characterizing the interaction of NH_3 molecules with the phthalocyanine between the indicated atoms).

Two points are located between the ammonia nitrogen atom and the non-peripheral hydrogen atoms of ZnPc-1py (BCP1 and BCP3, BCP4 and BCP6, BCP7 and BCP9, BCP10 and BCP12), while one point is between one of the NH_3 hydrogen atoms and the bridging nitrogen atom of ZnPc-1py (BCP2, BCP5, BCP8, BCP11).

It was previously shown [64] that, when the hydrogen bonds were formed, the values of $\rho(\mathbf{r})$ and $\nabla^2\rho(\mathbf{r})$ at the corresponding critical points should be in the ranges of 0.013–0.236 e/Å^3 and 0.578–3.350 e/Å^5, respectively. The values of the electron density and its Laplacian obtained by us fully satisfy these requirements (Table 3). Thus, it can be concluded that the attachment of the ammonia molecules to the side atoms of the phthalocyanines occurs due to the formation of exclusively hydrogen bonds, which is also evidenced by the values of E_b (Table 2).

Table 3. Values of $\rho(\mathbf{r})$ and $\nabla^2\rho(\mathbf{r})$ at bond critical points characterizing the interaction of four NH_3 molecules with the ZnPc-1py molecule and effective charges q of the corresponding hydrogen atoms of phthalocyanine.

BCP	Atoms	$\rho(\mathbf{r})$, e/Å^3	$\nabla^2\rho(\mathbf{r})$, e/Å^5	q, e
1	N1-H1	0.146	1.602	0.148
2	N2-H2	0.117	1.162	-
3	N1-H3	0.096	1.050	0.051
4	N3-H4	0.140	1.543	0.106
5	N4-H5	0.129	1.270	-
6	N3-H6	0.098	1.069	0.046
7	N5-H7	0.137	1.527	0.107
8	N6-H8	0.125	1.238	-
9	N5-H9	0.100	1.092	0.047
10	N7-H10	0.138	1.530	0.107
11	N8-H11	0.126	1.250	-
12	N7-H12	0.099	1.082	0.048

Thus, this fact allowed us to explain the experimental observations. If strong covalent bonds were formed as a result of the interaction of the NH_3 molecules with phthalocyanine, the desorption process would be difficult, and the sensor response would be irreversible. In this case, the changes in the electronic structure of the

CNT(10,0)/ZnPc-*x*py hybrids would be more significant due to the hybridization of the molecular orbitals, and the change in the energy of the impurity band would not be limited to hundredths of eV. Due to the weakness of these interactions, significant changes in the electronic structure of the CNT(10,0)/ZnPc-*x*py hybrids are not observed. In this regard, hydrogen bonds, which occupy an intermediate position between covalent and dispersion interactions, are the most suitable for explaining the phenomena observed in the experiments to study the sensor response of the CNT(10,0)/ZnPc-*x*py hybrid layers to ammonia, namely, its appearance and reversibility.

In ZnPc-1py/4NH_3, the total Mulliken charge of the atoms of the oxypyrene substituent is -0.044*e*; that is, the substituent pulls the electron density onto itself. As a result, it can be seen that the H1 atom (Figure 4) has the largest positive charge q among all the phthalocyanine hydrogen atoms involved in the formation of the hydrogen bonds with the NH_3 molecules. As a consequence, the values of $\rho(\mathbf{r})$ and $\nabla^2\rho(\mathbf{r})$ in BCP1 between this atom and the nitrogen atom N1 of ammonia are the largest when compared with the other indicated bond critical points (Table 3). This is what determines the highest bond strength of the NH_3 molecule in position 4 of the ZnPc-1py/4NH_3 structure (Figure 2, Table 2).

Thus, the effect of the oxypyrene substituents is to polarize the phthalocyanine molecule and, in particular, the side atoms with which ammonia interacts. As a result, the strength of the interaction of NH_3 with the ZnPc-*x*py molecules bearing the oxypyrene substituents is higher than in the case of ZnPc-0py without the substitutes. Stronger binding of the NH_3 molecules has a stronger effect on the electronic structure of phthalocyanine. This leads to a greater shift of the impurity band downward in energy in the CNT(10,0)/ZnPc-*x*py hybrids during ammonia adsorption with an increase in the number of oxypyrene substituents x in ZnPc-*x*py.

4. Conclusions

Quantum chemical calculations of the geometric and electronic structure of periodic hybrid compounds representing carbon nanotubes (10.0) with zinc phthalocyanine molecules on their surface have been carried out. Zinc phthalocyanines ZnPc-*x*py (x=0, 1, 2, 4) differed from each other in the number of oxypyrene substituents in the tetrapyrrole macrocycle. It was found, as a result of the calculations, that, in these hybrids, an impurity band formed by the orbitals of the phthalocyanine atoms was located in the band gap of the carbon nanotube. The electrons of this level do not directly participate in electric conduction; however, due to thermal excitation, they can pass into the conduction band. The probability of this transition is determined by the difference between the energies of the impurity band and the conduction band bottom. With an increase in the number of oxypyrene substituents, this difference decreases. The interaction of the ammonia molecules with the side phthalocyanine atoms on the surface of a carbon nanotube occurs through the formation of hydrogen bonds. As a result, the energy of the impurity band decreases. Consequently, the thermal population of the conduction band decreases. This explains the occurrence of the sensor response of the considered hybrid materials to ammonia, which is manifested as a decrease in electrical conductivity during the adsorption of gas molecules. Such interaction of ammonia through the formation of weak hydrogen bonds can cause the reversibility of the sensor response.

The strength of the bonds between the ammonia and phthalocyanine molecules increases with an increase in the number of oxypyrene substituents. As a result, the decrease in the energy of the impurity band becomes more significant, which leads to a more noticeable decrease in the thermal population of the conduction band. This may explain the higher value of the sensor response of the hybrids containing the larger number of oxypyrene substituents in the zinc phthalocyanine macrocycle, which was observed experimentally in our previous work, since, in this case, the decrease in electrical conductivity during adsorption of the same amount of ammonia molecules is more significant.

Author Contributions: Conceptualization, P.K. and T.B.; methodology, P.K. and T.B.; software, P.K.; validation, P.K., D.K. and A.F.; formal analysis, P.K. and A.F.; investigation, P.K. and V.I.; writing—original draft preparation, P.K., V.I. and T.B.; writing—review and editing, P.K., D.K. and T.B.; visualization, P.K.; supervision, T.B.; funding acquisition, D.K. All authors have read and agreed to the published version of the manuscript.

Funding: Studies of periodic hybrid materials were performed under the financial support of the Russian Science Foundation (grant 20-12-00175). Studies of the interaction parameters of ammonia molecules with phthalocyanines were carried out under the financial support of the Ministry of Science and Higher Education of the Russian Federation (N 121031700314-5).

Institutional Review Board Statement: Not applicable.

Informed Consent Statement: Not applicable.

Data Availability Statement: Not applicable.

Conflicts of Interest: The authors declare no conflict of interest.

References

1. Zaporotskova, I.V.; Boroznina, N.P.; Parkhomenko, Y.N.; Kozhitov, L.V. Carbon nanotubes: Sensor properties. A review. *Mod. Electron. Mater.* **2016**, *2*, 95–105.
2. Norizan, M.N.; Siti Zulaikha, N.D.; Norhana, A.B.; Syakir, M.I.; Norli, A. Carbon nanotubes-based sensor for ammonia gas detection—An overview. *Polimery* **2021**, *66*, 175–186.
3. Giordano, C.; Filatrella, G.; Sarno, M.; Di Bartolomeo, A. Multi-walled carbon nanotube films for the measurement of the alcoholic concentration. *Micro Nano Lett.* **2019**, *14*, 304–308.
4. Le, X.V.; Luu, T.L.A.; Nguyen, H.L.; Nguyen, C.T. Synergistic enhancement of ammonia gas-sensing properties at low temperature by compositing carbon nanotubes with tungsten oxide nanobricks. *Vacuum* **2019**, *168*, 108861.
5. Vu, T.D.; Cong, T.N.; Huu, B.L.; Duc, C.N.; Huu, L.N. Surface-modified carbon nanotubes for enhanced ammonia gas sensitivity at room temperature. *J. Nanosci. Nanotechnol.* **2019**, *19*, 7447–7451.
6. Norizan, M.N.; Moklis, M.H.; Ngah Demon, S.Z.; Halim, N.A.; Samsuri, A.; Mohamad, I.S.; Knight, V.F.; Abdullah, N. Carbon nanotubes: Functionalisation and their application in chemical sensors. *RSC Adv.* **2020**, *10*, 43704–43732.
7. Saxena, S.; Srivastava, A.K.; Srivastava, R.; Kheraj, V. Metal-phthalocyanine functionalized CNTs sensor for chloroform series. *Eur. J. Eng. Sci. Technol.* **2019**, *2*, 71–80.
8. Ansari, N.; Lone, M.Y.; Shumaila; Ali, J.; Zulfequar, M.; Husain, M.; Islam, S.S.; Husain, S. Trace level toxic ammonia gas sensing of single-walled carbon nanotubes wrapped polyaniline nanofibers. *J. Appl. Phys.* **2020**, *127*, 044902.
9. Bouanis, F.Z.; Bensifia, M.; Florea, I.; Mahouche-chergui, S.; Carbonnier, B.; Grande, D.; Léonard, C.; Yassar, A.; Pribat, D. Non-covalent functionalization of single walled carbon nanotubes with Fe-/Co-porphyrin and Co-phthalocyanine for field-effect transistor applications. *Org. Electron.* **2021**, *96*, 106212.
10. Polyakov, M.S.; Basova, T.V. Hybrid materials of zinc (II) tetra-tert-butylphthalocyanine and zinc (II) tetra-tert-butylnaphthalocyanine with single walled carbon nanotubes: Structure and sensing propertie. *Macroheterocycles* **2017**, *10*, 31–36.
11. Kaya, E.N.; Tuncel, S.; Basova, T.; Banimuslem, H.; Hassan, A.; Gürek, A.G.; Ahsen, V.; Durmuş, M. Effect of pyrene substitution on the formation and sensor properties of phthalocyanine-single walled carbon nanotube hybrids. *Sens. Actuators B. Chem.* **2014**, *199*, 277–283.
12. Krasnov, P.O.; Ivanova, V.N.; Basova, T.V. Carbon nanotubes functionalized with Zinc (II) phthalocyanines: Effect of the expanded aromatic system and aromatic substituents on the binding energy. *Appl. Surf. Sci.* **2021**, *547*, 149172.
13. Sharma, A.K.; Mahajan, A.; Bedi, R.K.; Kumar, S.; Debnath, A.K.; Aswal, D.K. Non-covalently anchored multi-walled carbon nanotubes with hexa-decafluorinated zinc p hthalocyanine as ppb level chemiresistive chlorine sensor. *Appl. Surf. Sci.* **2018**, *427*, 202–209.
14. Saini, R.; Mahajan, A.; Bedi, R.K.; Aswal, D.K.; Debnath, A.K. Room temperature ppb level Cl_2 detection and sensing mechanism of highly selective and sensitive phthalocyanine nanowires. *Sens. Actuators B. Chem.* **2014**, *203*, 17–24.
15. Chia, L.S.; Du, Y.H.; Palale, S.; Lee, P.S. Interaction of copper phthalocyanine with nitrogen dioxide and ammonia investigation using X-ray absorption spectroscopy and chemiresistive gas measurements. *ACS Omega* **2019**, *4*, 10388–10395.
16. Wang, B.; Wang, X.; Li, X.; Guo, Z.; Zhou, X.; Wu, Y. The effects of amino substituents on the enhanced ammonia sensing performance of PcCo/rGO hybrids. *RSC Adv.* **2018**, *8*, 41280–41287.
17. Gai, S.; Wang, B.; Wang, X.; Zhang, R.; Miao, S.; Wu, Y. Ultrafast NH_3 gas sensor based on phthalocyanine-optimized non-covalent hybrid of carbon nanotubes with pyrrole. *Sens. Actuators B. Chem.* **2022**, *357*, 131352.
18. Kang, D.; Wang, B.; Wang, X.; Li, Y.; Chen, Z.; He, C.; Wu, Y. Stably dispersed metallophthalocyanine noncovalently bonded to multiwalled carbon nanotubes for ammonia sensing at room temperature. *Sens. Actuators B. Chem.* **2017**, *246*, 262–270.
19. Prasongkit, J.; Tangsukworakhun, S.; Jaisutti, R.; Osotchan, T. Highly sensitive and selective sensing of acetone and hydrogen sulfide using metal phthalocyanine—carbon nanotube hybrids. *Appl. Surf. Sci.* **2020**, *532*, 147314.

20. Basiuk, E.V.; Huerta, L.; Basiuk, V.A. Noncovalent bonding of 3d metal (II) phthalocyanines with single-walled carbon nanotubes: A combined DFT and XPS study. *Appl. Surf. Sci.* **2019**, *470*, 622–630.
21. Mendoza-Domínguez, C.U.; Basiuk, V.A. Adsorption of yttrium bisphthalocyanine on pristine and defect-contaning graphene models: A DFT study. *Diam. Relat. Mater.* **2022**, *126*, 109051.
22. Li, Y.; Wang, B.; Yu, Z.; Zhou, X.; Kang, D.; Wu, Y.; Chen, Z.; He, C.; Zhou, X. The effects of central metals on ammonia sensing of metallophthalocyanines covalently bonded to graphene oxide hybrids. *RSC Adv.* **2017**, *7*, 34215–34225.
23. Ridhi, R.; Neeru; Gautam, S.; Saini, G.S.S.; Tripathi, S.K.; Rawat, J.S.; Jha, P. Study of the effect of orbital on interaction behaviour of SWCNT-metal phthalocyanines composites with ammonia gas. *Sens. Actuators B. Chem.* **2021**, *337*, 129767.
24. Dasari, B.S.; Taube, W.R.; Agarwal, P.B.; Rajput, M.; Kumar, A.; Akhtar, J. Room temperature single walled carbon nanotubes (SWCNT) chemiresistive ammonia gas sensor. *Sens. Transducers* **2015**, *190*, 24–30.
25. Nikolic, M.V.; Milovanovic, V.; Vasiljevic, Z.Z.; Stamenkovic, Z. Semiconductor gas sensors: Materials, technology, design, and application. *Sensors* **2020**, *20*, 6694.
26. Kaya, E.N.; Basova, T.; Polyakov, M.; Durmuş, M.; Hassan, A. Hybrid materials of pyrene substituted phthalocyanines with single-walled carbon nanotubes: Structure and sensing properties. *RSC Adv.* **2015**, *5*, 91855–91862.
27. Polyakov, M.S.; Basova, T.V.; Göksel, M.; Şenocak, A.; Demirbaş, E.; Durmuş, M.; Kadem, B.; Hassan, A. Effect of covalent and non-covalent linking of zinc(II) phthalocyanine functionalised carbon nanomaterials on the sensor response to ammonia. *Synth. Met.* **2017**, *227*, 78–86.
28. Guo, Z.; Wang, B.; Wang, X.; Li, Y.; Gai, S.; Wu, Y.; Cheng, X. A high-sensitive room temperature gas sensor based on cobalt phthalocyanines and reduced graphene oxide nanohybrids for the ppb-levels of ammonia detection. *RSC Adv.* **2019**, *9*, 37518–37525.
29. Wu, H.; Chen, Z.M.; Zhang, J.L.; Wu, F.; He, C.H.; Ren, Z.Y.; Wu, Y.Q. Manipulating polyaniline fibrous networks by doping tetra-β-carboxyphthalocyanine cobalt(II) for remarkably enhanced ammonia sensing. *Chem. Mater.* **2017**, *29*, 9509–9517.
30. Tai, H.; Duan, Z.; He, Z.; Xian, L.; Xu, J.; Liu, B.; Jiang, Y. Enhanced ammonia response of Ti_3C_2Tx nanosheets supported by TiO_2 nanoparticles at room temperature. *Sens. Actuators B. Chem.* **2019**, *298*, 126874.
31. Zhang, D.; Jiang, C.; Li, P.; Sun, Y. Layer-by-Layer Self-assembly of Co_3O_4 Nanorod-Decorated MoS_2 Nanosheet-Based Nanocomposite toward High-Performance Ammonia Detection. *ACS Appl. Mater. Interfaces* **2017**, *9*, 6462–6471.
32. Ridhi, R.; Singh, S.; Saini, G.S.S.; Tripathi, S.K. Comparison of interaction mechanisms of copper phthalocyanine and nickel phthalocyanine thin films with chemical vapours. *J. Phys. Chem. Solids* **2018**, *115*, 119–126.
33. Liang, X.; Chen, Z.; Wu, H.; Guo, L.; He, C.; Wang, B.; Wu, Y. Enhanced NH_3-sensing behavior of 2,9,16,23-tetrakis(2,2,3,3-tetrafluoropropoxy) metal(II) phthalocyanine/multi-walled carbon nanotube hybrids: An investigation of the effects of central metals. *Carbon* **2014**, *80*, 268–278.
34. Cao, Z.; Chen, Q.; Lu, Y.; Liu, H.; Hu, Y. Density functional theory study on the interaction between metalloporphyrins and NH_3. *Int. J. Quantum Chem.* **2012**, *113*, 1137–1146.
35. Baggio, A.R.; Machado, D.F.S.; Carvalho-Silva, V.H.; Paterno, L.G.; de Oliveira, H.C.B. Rovibrational spectroscopic constants of the interaction between ammonia and metallo-phthalocyanines: A theoretical protocol for ammonia sensor design. *Phys. Chem. Chem. Phys.* **2017**, *19*, 10843–10853.
36. Rana, M.K.; Sinha, M.; Panda, S. Gas sensing behavior of metal-phthalocyanines: Effects of electronic structure on sensitivity. *Chem. Phys.* **2018**, *513*, 23–24.
37. Kaya, E.N.; Şenocak, A.; Klyamer, D.D.; Demirbaş, E.; Basova T.V.; Durmuş M. Ammonia sensing performance of thin films of cobalt(II) phthalocyanine bearing fluorinated substituents. *J. Mater. Sci: Mater. Electron* **2019**, *30*, 7543–7551.
38. Ivanova, V.; Klyamer, D.; Krasnov, P.; Kaya, E.N.; Kulu, İ.; Kostakoglu, S.T.; Durmuş, M.; Basova, T. Hybrid materials based on pyrene-substituted metallo phthalocyanines as sensing layers for ammonia detection: Effect of the number of pyrene substituents. *Sens. Actuators B. Chem.* **2023**, *375*, 132843.
39. Elstner, M.; Porezag, D.; Jungnickel, G.; Elsner, J.; Haugk, M.; Frauenheim, T.; Suhai, S.; Seifert, G. Self-consistent-charge density-functional tight-binding method for simulations of complex materials properties. *Phys. Rev. B* **1998**, *58*, 7260–7268.
40. Hourahine, B.; Aradi, B.; Blum, V.; Bonafé, F.; Buccheri, A.; Camacho, C.; Cevallos, C.; Deshaye, M.Y.; Dumitric, T.; Dominguez, A.; et al. DFTB+, a software package for efficient approximate density functional theory based atomistic simulations. *J. Chem. Phys.* **2020**, *152*, 124101.
41. Lu, X.; Gaus, M.; Elstner, M.; Cui, Q. Parametrization of DFTB3/3OB for magnesium and zinc for chemical and biological applications. *J. Phys. Chem. B* **2015**, *119*, 1062–1082.
42. Gaus, M.; Goez, A.; Elstner, M. Parametrization and benchmark of DFTB3 for organic molecules. *J. Chem. Theory Comput.* **2013**, *9*, 338–354.
43. Grimme, S.; Ehrlich, S.; Goerigk, L. Effect of the damping function in dispersion corrected density functional theory. *J. Comput. Chem.* **2011**, *32*, 1456–1465.
44. Grimme, S.; Antony, J.; Ehrlich, S.; Krieg, H. A consistent and accurate ab initio parametrization of density functional dispersion correction (DFT-D) for the 94 elements H-Pu. *J. Chem. Phys.* **2010**, *132*, 154104.
45. Krasnov, P.O.; Basova, T.V.; Hassan, A. Interaction of metal phthalocyanines with carbon zigzag and armchair nanotubes with different diameters. *Appl. Surf. Sci.* **2018**, *457*, 235–240.
46. Monkhorst, H.J.; Pack, J.D. Special points for Brillonin-zone integrations. *Phys. Rev. B* **1976**, *13*, 5188–5192.

47. Becke, A.D. Density-functional exchange energy approximation with correct asymptotic behavior. *Phys. Rev. A* **1988**, *38*, 3098–3100.
48. Perdew, J.P. Density functional approximation for the correlation energy of the inhomogeneous electron gas. *Phys. Rev. B* **1986**, *33*, 8822–8824.
49. Weigend, F.; Ahlrichs, R. Balanced basis sets of split valence, triple zeta valence and quadruple zeta valence quality for H to Rn: Design and assessment of accuracy. *Phys. Chem. Chem. Phys.* **2005**, *7*, 3297–3305.
50. Neese, F. The ORCA program system. *WIREs Comput. Mol. Sci.* **2012**, *2*, 73–78.
51. Neese, F. Software update: The ORCA program system, version 4.0. *WIREs Comput. Mol. Sci.* **2017**, *8*, e1327.
52. Baerends, E.J.; Ellis, D.E.; Ros, P. Self-consistent molecular Hartree-Fock-Slater calculations I. The computational procedure. *J. Chem. Phys.* **1973**, *2*, 41–51.
53. Dunlap, B.I.; Connolly, J.W.D.; Sabin, J.R. On some approximations in applications of Xα theory. *J. Chem. Phys.* **1979**, *71*, 3396–3402.
54. Van Alsenoy, C. Ab initio calculations on large molecules: The multiplicative integral approximation. *J. Comp. Chem.* **1988**, *9*, 620–626.
55. Kendall, R.A.; Früchtl, H.A. The impact of the resolution of the identity approximate integral method on modern ab initio algorithm development. *Theor. Chem. Acc.* **1997**, *97*, 158–163.
56. Eichkorn, K.; Treutler, O.; Öhm, H. Auxiliary basis sets to approximate Coulomb potentials. *Chem. Phys. Lett.* **1995**, *240*, 283–290.
57. Eichkorn, K.; Weigend, F.; Treutler, O. Auxiliary basis sets for main row atoms and transition metals and their use to approximate Coulomb potentials. *Theor. Chem. Acc.* **1997**, *97*, 119–124.
58. Weigend, F. Accurate Coulomb-fitting basis sets for H to Rn. *Phys. Chem. Chem. Phys.* **2006**, *8*, 1057–1065.
59. Dunning, T.H., Jr. Gaussian basis sets for use in correlated molecular calculations. I. The atoms boron through neon and hydrogen. *J. Chem. Phys.* **1989**, *90*, 1007–1023.
60. Bader, R.F.W.; Essén, H. The characterization of atomic interactions. *J. Chem. Phys.* **1984**, *80*, 1943–1960.
61. Bader, R.F.W. A quantum theory of molecular structure and its applications. *Chem. Rev.* **1991**, *91*, 893–928.
62. Bader, R.F.W. *Atoms in Molecules: A Quantum Theory;* Oxford University Press: New York, NY, USA, 1994.
63. Todd, A.; Keith, T.K. *AIMAll,* version 19.10.12; Gristmill Software: Overland Park, KS, USA, 2019. Available online: aim.tkgristmill.com (accessed on 24 October 2022).
64. Bushmarinov, I.S.; Lyssenko, K.A.; Antipin, M.Y. Atomic energy in the 'Atoms in Molecules' theory and its use for solving chemical problems. *Russ. Chem. Rev.* **2009**, *78*, 283–302.